

Structural and functional analysis of a novel psychrophilic β -mannanase from *Glaciozyma antarctica* PI12

Sepideh Parvizpour · Jafar Razmara ·
Aizi Nor Mazila Ramli · Rosli Md Illias ·
Mohd Shahir Shamsir

Received: 7 February 2014 / Accepted: 12 May 2014 / Published online: 22 May 2014
© Springer International Publishing Switzerland 2014

Abstract The structure of a novel psychrophilic β -mannanase enzyme from *Glaciozyma antarctica* PI12 yeast has been modelled and analysed in detail. To our knowledge, this is the first attempt to model a psychrophilic β -mannanase from yeast. To this end, a 3D structure of the enzyme was first predicted using a threading method because of the low sequence identity (<30 %) using MODELLER9v12 and simulated using GROMACS at varying low temperatures for structure refinement. Comparisons with mesophilic and thermophilic mannanases revealed that the psychrophilic mannanase contains longer loops and shorter helices, increases in the number of aromatic and hydrophobic residues, reductions in the number of hydrogen bonds and salt bridges and numerous amino acid substitutions on the surface that increased the flexibility and its efficiency for catalytic reactions at low temperatures.

Keywords Mannanase · Psychrophiles · Cold adaptation · Structure prediction · Flexibility

Introduction

Psychrophiles are cold loving microorganisms that have adapted to live in permanently cold environments that are close to the freezing point of water. These microorganisms synthesise psychrophilic enzymes with high catalytic efficiencies at cold temperatures. This adaptation requires an adjustment in various cellular components, including the membrane, protein synthesis machinery, energy-generating systems, and other physicochemical characteristics. Enzymes from psychrophiles are supposed to be structurally more flexible than their mesophilic and thermophilic counterparts. This structural flexibility improves the ability of the protein to undergo conformational changes during catalysis and creates an enhanced catalytic efficiency at low temperature with an inherent decrease in the chemical reaction rates. This establishes the proper plasticity around the active site that is important for the thermolability of enzymes to obtain high catalytic efficiencies at low temperatures [1]. These specific characteristics of psychrophilic enzymes provide potential industrial applications in biotechnology and related fields [2].

Mannans and heteromannans are important biopolymers. Endo-1,4- β -D-mannanase (β -mannanase; E.C. 3.2.1.78) is the key depolymerising mannan-degrading enzyme that catalyses the random hydrolysis of β -D-1,4-mannopyranosyl linkages within the main chain of galactomannan, glucomannan, galactoglucomannan and mannan [3]. This enzyme plays an important role in the digestion of hemicelluloses. A majority of the identified β -mannanases are synthesised in bacteria and fungi [4, 5]. β -mannanases have also been isolated from plants, algae and mollusks

S. Parvizpour · M. S. Shamsir (✉)
Bioinformatics Research Group, Faculty of Bioscience and
Medical Engineering, Universiti Teknologi Malaysia,
Johor Bahru, Malaysia
e-mail: shahir@fbb.utm.my

J. Razmara
Department of Computer Science, Faculty of Mathematical
Sciences, University of Tabriz, Tabriz, Iran

A. N. M. Ramli
Faculty of Industrial Sciences & Technology, Universiti
Malaysia Pahang, Kuantan, Malaysia

R. Md Illias
Department of Bioprocess Engineering, Faculty of Chemical
Engineering, Universiti Teknologi Malaysia, Johor Bahru,
Malaysia

[6–8]. These enzymes commonly fold into a classic $(\beta/\alpha)_8$ -barrel and hydrolyse the glycosidic bond by a double displacement or “retaining” mechanism [9]. Interest in the potential applications of β -mannanases has increased in several industrial processes because of their important role in the bioconversion of lignocelluloses, one of the most abundant reusable resources in nature [10]. β -mannanases are used in the production of animal feed [11] and laundry detergents [12]. The enzymes also have a wide commercial application in the pulp, paper, food, pharmaceutical, and energy industries [11–14].

Because of the structural complexity, the degradation of mannans requires several hydrolytic enzymes. The mannan-degrading enzymes include β -mannanases (1,4- β -D-mannan mannohydrolase, EC 3.2.1.78), β -mannosidases (1,4- β -D-mannopyranoside hydrolase, EC 3.2.1.25), β -glucosidases (1,4- β -Dglucoside glucohydrolase), and esterases [5]. β -mannanase is considered the main enzyme in degradation because of its wide distribution in microorganisms. According to a sequence similarity analysis, the enzyme has been categorised in family 5, 26 and 113 of glycoside hydrolases (see the CAZy site; <http://www.cazy.org>) [15] which are members of clan GH-A of glycosyl hydrolases [16]. The GH5 is the largest family and includes both β -mannanases and β -mannosidases. Additionally, GH5 consists of bacterial and eukaryotic endo- β -d-1,4-mannanases (EC 3.2.1.78), endoglucanases (EC 3.2.1.4) and exo-1,3-glycanases. Several solved 3D crystal structures are available for β -mannanases in GH5 (PDB IDs: 2WHJ [15], 4AWE [17], 3JUG [18], 3PZ9 [19], 1WKY [20], 1QNR [21], 2C0H [22], and 1RH9 [23]). The optimal temperature ranges for these enzymes are reported to be mesophilic to moderately thermophilic [15, 17–19]. However, β -mannanase from the psychrophilic organisms of bacterial *Flavobacterium* [24] and blue mussel *Mytilus edulis* [22] have been isolated. Whereas mesophilic β -mannanases are generally active at higher temperatures greater than 50 °C, psychrophilic β -mannanases are significantly active under low temperatures. This activity of psychrophilic β -mannanases is useful to reduce the viscosity of food materials that complicates food processing at low temperatures. Food processing at lower temperatures is preferential to avoid deteriorating food materials [18].

Several studies have characterised β -mannanase from different microorganisms such as for *Paenibacillus* sp. [14], *Lycopersicon esculentum* [23] and *Aspergillus niger* [25]. This present investigation is the first study of the sequence and structural characterisation of a psychrophilic yeast β -mannanase enzyme. The aim of this study is to model the structure of a novel β -mannanase from *Glaciozyma Antarctica* PI12 [26] belonging to family 5 of glycosyl hydrolases. The proposed model of the enzyme was also structurally analysed and simulated using a molecular dynamic simulation. To clarify the potential

cold-adaptations of the β -mannanase enzyme, a comparative study was performed between the primary sequence and the predicted structure of the new β -mannanase enzyme and similar mesophilic and thermophilic β -mannanases. Finally, several analyses were performed to provide useful details on the thermolability of this enzyme.

Materials and methods

Sequence retrieval and analysis

The full-length gene of the novel β -mannanase, PMAN, was isolated from the cDNA library of *G. Antarctica* PI12. A total of 3 μ g of mRNA was used to construct a cDNA library using the CloneMiner cDNA Library Construction Kit (Invitrogen, USA) following the manufacturer's protocol. PSI-BLAST [27] and BLAST-PDB [28] was used to analyse the amino acid sequence of the isolated gene (549 residues). The SUPER-FAMILY HMM server [29] was utilised to identify conserved domains and possible families of the protein.

Building the 3D-model

Because of the low sequence identity of the alignment (less than 30 %), a threading method was utilised to build a 3D-model for the protein. The amino acid sequence was submitted to the library of known folds using PSI-BLAST [27], Modlink+ [30], HHpred [31], mGenThreader [32], and Phyre2 [33] to screen for potential available structural templates based on a threading method. The most common model was selected from the output list of the servers, and the selected sequence alignments from each server were given as the input to build 3D-models using MODELLER9v12 [34]. For each alignment, 50 models were generated in MODELLER9v12, and the model with the lowest DOPE score and/or the highest GA341 score was selected. Finally, the best model from the chosen models was selected based on the highest value of the TM-score [35] that is calculated by the TM-align program. The TM-score is a more significant score to assess the quality of an alignment because it balances the root mean square deviation (RMSD) and the length of alignment. The score is widely used in the evaluation of models. The resulting 3D-model was assessed by different tools including VERIFY-3D [36], PRO-CHECK [37], ERRAT [38], and ProSA-web [39].

Molecular dynamic (MD) simulation

The model was subjected to energy minimisation by the GROMACS 4.6.3 software package. The resulting model

was refined with a molecular dynamics simulation that was performed using the GROMOS 96 [40] force field. Additionally, to examine the structural stability of PMAN at three different temperatures including a low temperature (273 K or 0 °C), the working temperature (288 K or 15 °C) as the optimum temperature, and a moderate temperature (300 K or 27 °C) a molecular dynamics simulation was performed. The model protein was first placed into a suitably sized simulation cubic box and solvated with simple point-charge water molecules. In addition, 7 Na⁺ counter ions were added to neutralise the negative charge. The entire system was minimised using the steepest descent of 400 steps. To obtain the equilibrium geometry at 288 K and 1 atm, the system was heated at a weak temperature ($t = 0.1$ ps) and pressure ($t = 0.5$ ps) by employing Berendsen algorithms. All simulations were performed at a constant temperature and pressure with a non-bonded cut-off of 1.4 Å. The molecular dynamics simulation was performed for 10 ns at 288 K, LINCS was used to constrain the bond length, and the particle mesh Ewald method was employed for the electrostatic interactions. The integration time step was 2 fs, and the neighbour list was updated every fifth step using the grid option with a cut-off distance of 1.4 Å. A periodic boundary condition was used with a constant number of particles in the system, pressure, and temperature simulation criteria (NPT). During the simulation, every 1.0 ps of the actual frame was stored. The stabilised structure was taken from the trajectory of the system to determine the quality of the protein geometry and the structure folding reliability. Subsequently, the dynamic behaviour and the structural changes of the protein were analysed by calculating the RMSD. To investigate the structural stability of PMAN, the simulations were also calculated at three different temperatures: 273, 288 and 300 K. Simulations at these three different temperatures were expected to show a discernible MD stability profile. Finally, the RMSD and RMSF analysis were performed.

Cold adaptation analysis by structural comparison study

The cold adaptation of the resulting crystal structure of β -mannanase was analysed by a structural comparative study with a thermophilic β -mannanase from *Thermotoga petrophila* (3PZ9) [19] and mesophilic β -mannanases from *Podospira anserina* (3ZIZ) [41] and *L. esculentum* (1RH9) [23]. The ESBRI program was used to analyse salt bridges [42]. The DIANNA program was used to investigate disulphide bonds, and Accelrys DS studio 2.5 was applied to calculate hydrogen bonds and the accessible surface area. The graphical representation of the 3D-model was prepared in UCSF CHIMERA software [43].

Results and discussion

PMAN sequence analysis

The complete sequence of the β -mannanase has been deposited into the GenBank database under accession no. KJ775790. The sequence analysis study revealed that the psychrophilic PMAN protein exhibited a low similarity with all known β -mannanase structures in the PDB database. The consensus of all the software in Table 1 shows an efficient match of 38 % similarity and 24 % identity with the Endo-Beta-Mannanase from *L. Esculentum* (1RH9). The PSI-BLAST and SUPERFAMILY HMM library result identified the catalytic domain of PMAN as a cellulase and belonging to the TIM barrel family 5 of a glycosyl hydrolase.

3D-model prediction

Considering that the sequence analysis results showed a low identity percentage for the PMAN protein (24 %), we applied a threading method to recognize folds. The amino acid sequence of the PMAN protein was submitted to a set of known threading methods including PSI-BLAST, Modlink+, HHpred, mGenThreader, and Phyre2 and the results were evaluated as represented in Table 1. Comparing the threading results from Table 1, the catalytic domain of the endo-beta-mannanase from *L. Esculentum* (1RH9) appeared in the results of all servers and obtained the best score with a high identity and a low e-value. This protein was found to have the identical TIM barrel family as PMAN. Based on the sequence alignment results given by different servers, 1RH9 is a suitable template structure for PMAN. The 3PZ9 was the second choice because it was common among the templates proposed by the servers in Table 1. However, 3PZ9 has a lower reliability in the alignment than 1RH9 because 3PZ9 produces more insertions and deletions in the sequence-structure alignment. These insertions and deletions are catastrophic to the prediction of the 3D-structure. Accordingly, we chose 1RH9 as the template structure for PMAN.

Additionally, a study was performed on the consensus secondary structure of PMAN and 1RH9 to investigate the reliability of the constructed model. Figure 1 shows the alignment between PMAN and 1RH9 in the secondary structure and at the residue level as predicted by the HHpred server. Based on the figure, PMAN and 1RH9 aligned well for 8 α -helices and 8 β -strands. The alignment also consists of several structural differences and also two long gaps starting at residue number 409, 435 and 461. These differences will be discussed in the model analysis section.

Table 1 Top three proposed templates by different threading tools. 1RH9 obtained the best score including identity and e-value and was chosen as the template for PMAN protein

Server name	Template	Protein	Fold	Identity	E-value
PSI-BLAST	3pz9	Endo-1,4-beta-D-mannanase	Tim Barel	28 %	2e-18
	1rh9	Endo-beta-mannanase	Tim Barel	24 %	2e-14
	lqno	Beta-mannanase	Tim Barel	23 %	4e-07
Modlink+	1rh9	Endo-beta-mannanase	Tim Barel	20 %	1e-107
	lqnr	Beta-mannanase	Tim Barel	19 %	7e-89
	luuq	Exo-mannosidase	Tim Barel	14 %	7e-77
HHPred	1rh9	Endo-beta-mannanase	Tim Barel	23 %	1.1e-42
	luuq	Exo-mannosidase	Tim Barel	17 %	7.3e-42
	3ZIZ	Beta- 1,4-mannanase	Tim Barel	15 %	7.9e-42
mGenThreader	1rh9	Endo-beta-mannanase	Tim Barel	Not available	2e-11
	3ZIZ	Beta- 1,4-mannanase	Tim Barel	Not available	2e-11
	lqno	Beta-mannanase	Tim Barel	Not available	2e-11
Phyre2	luuq	Exo-mannosidase	Tim Barel	19 %	0
	luz4	Exo-mannosidase	Tim Barel	19 %	0
	1rh9	Endo-beta-mannanase	Tim Barel	26 %	0

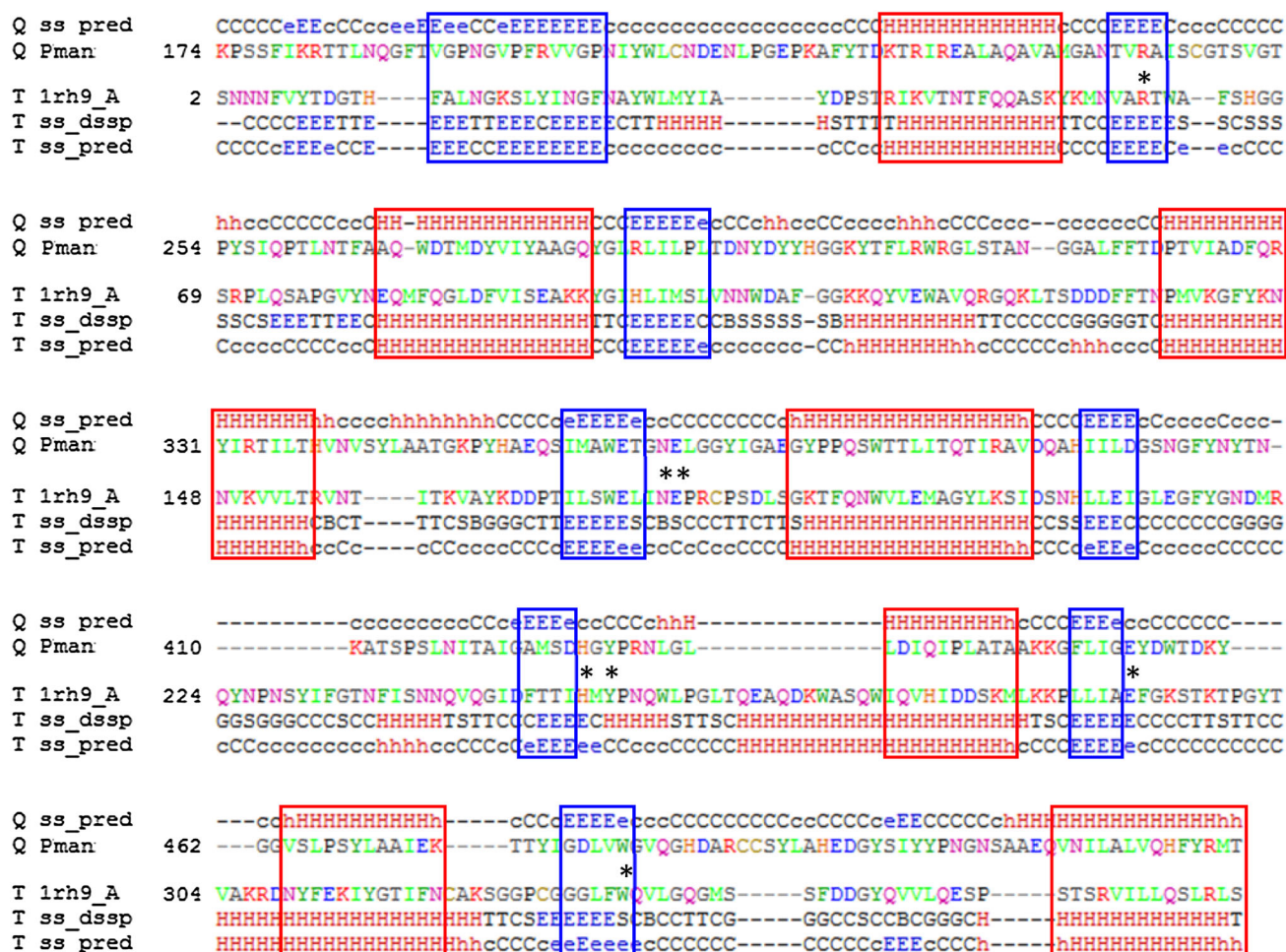
**Fig. 1** The alignment between PMAN and 1RH9 in secondary structure and residue levels predicted by HHpred server. The blue and red boxes show the aligned secondary structure alignments (helices and strands, respectively). The active sites are shown by star

Table 2 Evaluation of the best models created by MODELLER program for the alignments produced by different servers

Server name	Best model	RMSD	Length of alignment	TM-score
PSI-BLAST	32.pdb	1.30	292	0.90
Modlink+	9.pdb	0.98	323	0.90
HHPred	11.pdb	0.90	327	0.93
mGenThreader	18.pdb	0.89	331	0.89
Phyre2	38.pdb	0.86	330	0.86

Constructing the 3D-model

With the endo-beta-mannanase (1RH9) protein selected as the 3D-model for PMAN, different threading tools were utilised to create an alignment between the two proteins and the alignment were submitted to the MODELLER program. The MODELLER program is used to compare protein structure models based on an alignment between the query and template sequence as the input. This program automatically calculates a model that includes all of the non-hydrogen atoms using a technique known as the satisfaction of spatial restraints. The models satisfying the best objective function (the lowest DOPE and/or the highest GA341) from different alignment tools were selected and submitted to the TM-align program to evaluate the alignments based on a TM-score. This score ranges between 0 and 1; a higher score represents a better template, and a score above 0.4 is considered significant. The alignments were evaluated and ranked based on these score as shown in Table 2.

Based on the results in Table 2, the model created by HHpred obtained the best RMSD of 0.90 and TM-score of 0.93. Although the length of the alignment for this model is slightly shorter than the models produced by three other programs, this model displayed substantially lower RMSD and higher TM-scores than the other models. Therefore, we selected the HHpred generated model as the best model for the PMAN protein.

To minimise the energy level of the selected model and to exclude poor molecular contacts, the model was submitted to the GROMACS 4.6.3 software package. The resulting model was subjected to CHARM-22 in the Accelrys Discovery Studio 2.5 to refine the side-chains and loops.

Evaluation of the model

To assess the quality of the constructed 3D-model, several model evaluation tools were implemented. At first, we used the PROCHECK tool to investigate the backbone conformation based on a Psi/Phi Ramachandran plot. According to the results of PROCHECK, only two residues (≈ 1 %)

Table 3 Model evaluation summary using different tools

Model evaluation tool	Evaluation scheme	Obtained score	Normal range of the score
PROCHECK	The number of residues in allowed region based on Psi/Phi Ramachandran plot	99.60 %	>90 %
VERIFY3D	The number of residues having an average 3D-1D score above 0.2	85.68 %	>80 %
ERRAT	The overall quality for nonbonded atomic interactions	92.45 %	>50 %
ProSA-web	Model evaluation by calculating an overall quality score (z-score)	−4.43	NPS

NPS native protein size check whether the Z-score of the input structure is within the range of scores typically found for native proteins of similar size

were located in a disallowed region (ASN132, and TYR188). Additionally, 78.1 % of the residues were found in the most favourable region, and the rest of residues were located in the additional and generally allowed region (≈ 21 %). During the analysis of the results of VERIFY3D, 85.68 % of the residues had an average 3D–1D score above 0.2, whereas 10 % of the residues did not obtain this score. The quality of a constructed model is considered satisfactory if it obtains a VERIFY3D score above 80 % [36]. ERRAT is another tool that is used to assess the overall quality of the model for nonbonded atomic interactions by comparing the statistics of highly refined structures. The accepted range of the ERRAT score for a good model is above 50 %, and a higher score indicates a better quality [44]. The ERRAT score of the model was 92.45 % and is acceptable in the normal range. ProSA-web was the last tool that was used to evaluate the model by calculating an overall quality score. The model structure is supposed to be without errors if this score is in the normal range for native proteins. The z-score of the model was calculated to be −4.43; this value is considered to be within the normal range of scores for native proteins of a similar size. Table 3 shows a summary of the evaluation results.

Considering that the PMAN structure was constructed using a threading method with a low sequence identity (less than 30 %) and a low sequence similarity (less than 45 %), the overall scores obtained for the model using different evaluation tools are considered reasonable.

Analysis of the model

The 3D model of the PMAN protein is represented in Fig. 2. The structural features of the model are similar to

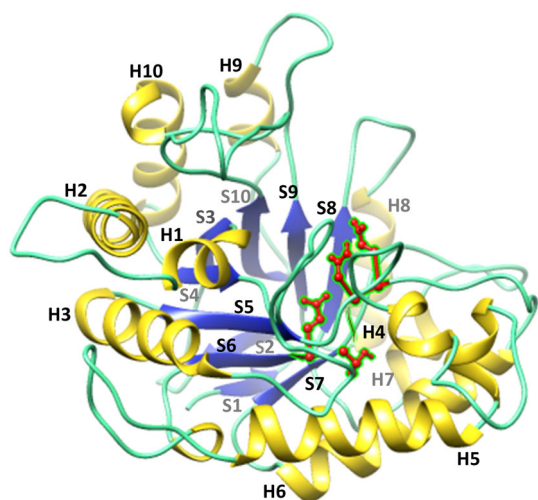


Fig. 2 3D-model of PMAN representing the secondary structure elements including α -helices, labelled H1–H10 and β -strands, labelled S1–S10. Two active site subsequences (NE and HGY) corresponding to residues 265–266 and 428–430 of PMAN are shown as *balls* and *sticks*

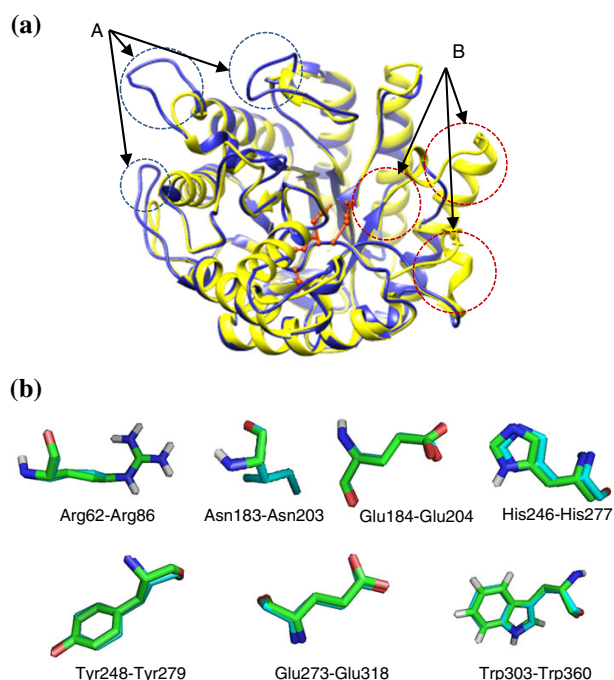


Fig. 3 **a** Superimposition of PMAN (*blue*) and its template, 1RH9 (*yellow*) in a cartoon representation. Longer loops in PMAN are indicated in three regions with *black circle* named A. Longer helices in 1RH9 are shown in three regions with *red circles* named B. **b** A close up view of the catalytic residue alignment of PMAN and 1RH9


those of other members in family 5 of glycosyl hydrolases. The PMAN structure consists of an alternating pattern of α -helices and β -strands in its catalytic domain and is considered as a TIM barrel fold. The TIM barrel structure has

been observed in most of the known mannanase structures [23] and is considered a common folding motif of family 5 mannanases. In the figure, the parallel β -strands that define the core of the enzyme are labelled as S1–S10, and the α -helices following each of these strands are labelled as H1–H10.

The superimposition between the PMAN 3D-model and 1RH9 as the selected template is represented in Fig. 3a. According to this superimposition, an RMSD of 2.198 Å and a 57 % coverage of the backbone atoms resulted from the superimposition. These values indicate a good alignment between these two structures. The catalytic regions of PMAN (Glu362–Glu366) and 1RH9 (Glu174–Glu178) are represented as balls and sticks. A close-up view of the catalytic regions of PMAN and 1RH9 is represented in Fig. 3b. The high accuracy of the constructed 3D-model is demonstrated in the conservation of the catalytic domain between PMAN and 1RH9 as the selected template and the identical structural assignments.

As the selected template, the endo-beta-mannanase (1RH9) structure (Fig. 4a) shows the classical $(\alpha/\beta)_8$ -barrel architecture similar to other members of family 5 glycosyl hydrolases. The structure has a roughly V-shaped groove similar to other β -mannanase structures that bind mannan [23]. In addition to this α/β -barrel domain (the TIM-barrel structure), the 1RH9 structure has additional α -helices and β -strands. These include three strands that are located near the N terminus forming a β -sheet that stacks against the central β -barrel at the opposite end of the active site. Three noncanonical helices surround the active site.

The overall structure of PMAN (Fig. 4b) is similar to that of the endo-beta-mannanase enzyme (1RH9) and is not described in detail here. However, a visual comparison of their structural superimposition in Fig. 3a and their pairwise alignment in Fig. 1 revealed two notable differences. The first important difference is the longer external loops on the surface of the PMAN molecule that comprises a gap with 1RH9 in three different positions of the alignment (as shown in the Fig. 3a). In addition, the structure for PMAN was also found to possess other longer loops which are absent in the 1RH9 structure. The second difference between the two structures is that the secondary structure of the 1RH9 molecule consists of three long helices that are overlapped with three shorter helices in the PMAN molecule. The PMAN molecule also shows a long gap at the beginning of their alignment as represented in Fig. 3a. These overlaps can also be observed in other pairs of helices and strands in which longer elements from 1RH9 have been superimposed with shorter elements from the PMAN structure. These two differences between the 1RH9 and PMAN structures are related because the longer helices in 1RH9 are replaced with longer loops in the PMAN structure. These longer loops may be responsible for the



Q ss_pred
Q Pman
180
T 2c0h_A
T ss_dssp
T ss_pred

Q ss_pred
Q Pman
257
T 2c0h_A
T ss_dssp
T ss_pred

Q ss_pred
Q Pman
332
T 2c0h_A
T ss_dssp
T ss_pred

Q ss_pred
Q Pman
386
T 2c0h_A
T ss_dssp
T ss_pred

Q ss_pred
Q Pman
450
T 2c0h_A
T ss_dssp
T ss_pred

Q ss_pred
Q Pman
491 (549)
T 2c0h_A
T ss_dssp
T ss_pred

Q ss_pred
Q Pman
329 (353)

same secondary structure except for two extra α -helices in 2C0H (green boxes) substituted by a longer loop and a gap in PMAN structure

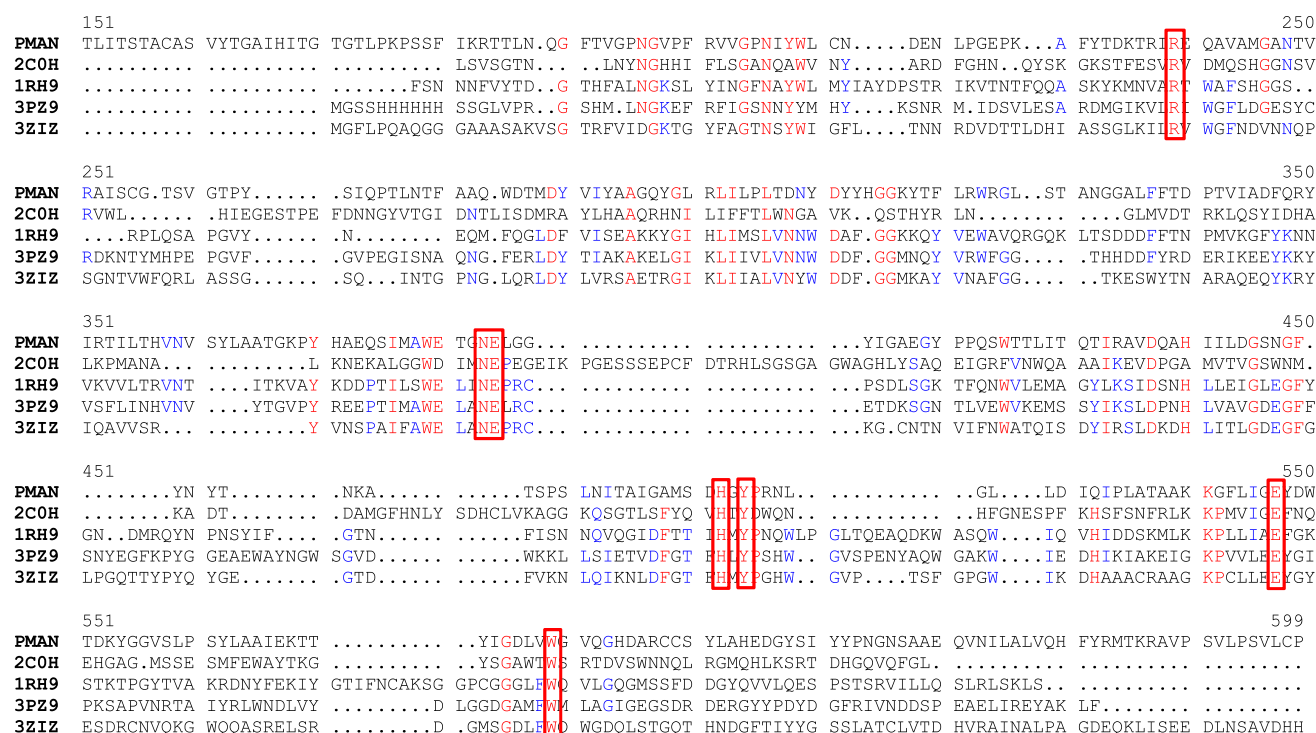


Fig. 6 Multiple sequence alignments of mannanases from *L. esculentum* (PDB code: 1RH9), thermophilic *T. petrophila* (PDB code: 3PZ9), mesophilic *P. anserina* (PDB code: 3ZIZ), and psychrophilic

G. antarctica (PMAN) and *Mytilus edulis* (2C0H). The conserved catalytic residues, Arg238, Asn374, Glu375, His455, Tyr457, Glu496 and Trp529 are shown by red boxes

flexibility of PMAN, contributing to cold adaptation at low temperatures. Longer surface loops increased the possible amplitude of the movement between the secondary structures and may decrease enzyme stability [45].

Additionally, the PMAN structure was compared with a psychrophilic β -mannanase from blue mussel *M. edulis* [22] (2C0H) to investigate additional structural differences. The alignment between these two structures is shown in Fig. 5. From this figure, the two structures have approximately the identical secondary structure except for two extra α -helices in 2C0H at the positions 121–129 and 243–250. The first helix is substituted by a longer loop whereas the second helix is missing in the PMAN structure. Moreover, the alignment shows a long gap in PMAN starting from position 370, this represents a long loop in 2C0H from 167 to 189. This gap is compensated by a loop in the PMAN structure at positions 340–351, this represents a gap in 2C0H starting from its position 149. The high structural similarity of these two psychrophilic proteins and the structural differences between PMAN and 1RH9 confirms the role of longer loops in the decrease of enzyme stability and increase in flexibility in psychrophilic β -mannanases. A similar study by Alvarez [46] revealed that the cold-adapted triosephosphate isomerase has more and longer loops connecting α -helices and β -sheets than homologs from mesophilic and thermophiles.

Comparative primary sequence analysis

A comparative study was performed to examine the psychrophilic features of PMAN based on the alignment of its sequence with different mannanases from *L. esculentum* (PDB code: 1RH9), psychrophilic *M. edulis* (2C0H), mesophilic *P. anserina* (PDB code: 3ZIZ) and thermophilic *T. petrophila* (PDB code: 3PZ9) mannanases. The sequence alignment revealed that the catalytic residues of the examined mannanases are conserved as represented in Fig. 6. According to previous studies, each psychrophilic enzyme has special alterations to its residues to adapt to cold environments. These changes typically increase the flexibility of the molecule, which in turn increases the catalytic efficiency of and reduces the stability at certain regions in a protein [47]. Analysing the multiple sequence alignment of PMAN with other psychrophilic, mesophilic and thermophilic mannanases in Fig. 6 highlights several notable substitutions in the amino acid residues of psychrophilic and non-psychrophilic proteins.

Proline is the first substituted amino acid that is closely related to the flexibility of a psychrophilic enzyme. The side chain of proline is covalently linked to the N atom of its backbone. This linkage reduces the conformational flexibility of the loop structure by restricting the rotation around the N–C $_{\alpha}$ bond [48]. Proline has a pyrrolidine ring

Table 4 Comparison of amino acid substitution between PMAN and mesophilic and thermophilic mannanases. The results obtained from multiple alignments represented in Fig. 6

Amino acid affecting thermostability/flexibility	Residues in mesophilic or thermophilic mannanase	Replacement in psychrophilic 2C0H	Replacement in psychrophilic PMAN	Residue No
Glycine (Destabilizing)	Pro, Ala	–	Gly	260
	His, Ser, Thr	–	Gly	333
	Asp, His, Lys	–	Gly	334
	Cys	Gly	Gly	387
	Asp	Ser	Gly	467
	Asp	Gly	Gly	542
	Ala, Glu	Gly	Gly	546
	Pro, Cys	Gly	Gly	556
Aromatic (stabilizing)	Asn, Ser, Gly	–	Phe	179
	Thr, Ser	–	Phe	190
	Leu, Val, Cys	His	Tyr	298
	Ser	His	Tyr	571
	Leu, Gly	–	Phe	581
Proline (destabilizing)	Pro, Ala	–	Gly	260
	Pro	Asn	Gln	266
	Pro	Lys	Gln	374
	Pro,Cys	Gly	Gly	556
	Pro, Asp	–	Asn	569
Proline (stabilizing)	Leu, Ile	–	Pro	194
	Phe, Ser, Thr	Tyr	Pro	204
	Asn, Ser, Thr	–	Pro	224
	Val, Phe, Ala	Tyr	Pro	362
	Ser, Lys	Pro	Gln	473
	Ileu	Pro	Pro	576
	Leu,Asn	Ser	Ala	243
Alanine, serin, threonine (destabilizing)	Glu, Lys, Ser	Ala	Ala	293
	Glu	Ser	Ala	345
	Asp, Asn	Ala	Ala	430
	Val,Leu,Ala	Ser	Thr	183
	His,Arg	–	Thr	191
	Ileu, Arg	Ser	Thr	229
	Asn, Glu, Gly	Thr	Thr	560

which restricts the potential conformations of the adjacent residues. Therefore, the stability and local rigidity of the molecule are increased because of the reduction of entropy in the molecular configuration and inhibition of chain flexibility [49]. Analysing the alignment in Fig. 6 revealed that proline has been substituted at positions 260, 266, 365, 504, and 560 of PMAN and 2C0H with other hydrophobic amino acids (asparagine, glycine, glutamine), as shown in Table 4. The presence of these hydrophobic residues plays an important role by increasing the flexibility of PMAN and 2C0H enzymes. Substitution of these hydrophobic surface residues highly destabilises the protein structure by constraining the entropy of the water molecule [50], in which it was found at positions 45, 260 and 365 on the surface of these molecules. Proline

substitutions in the loop regions enforce stabilising effects to generate flexibility on the substrate-binding cleft, which provides the ability to catalyse reactions in cold environments [45]. However, the PMAN and 2C0H structures consist of several proline residues (194, 204, 224, 353, 438, and 529) that are conserved with different residues in mesophilic and thermophilic mannanases. These replacements support the idea that there is an improved adaptation in the flexibility of different structural components of psychrophilic enzymes involved in the catalytic cycle or other parts of the molecule [48]. Additionally, to enable the optimal catalysis at low temperatures, the molecular structure requires a proper balance between its flexibility and rigidity to maintain its 3D conformation in cold environments.

Aromatic residues are another important substitution in the PMAN and 2C0H chains that cause the stability of the molecule in proper regions. These replacements are located at positions 179, 190, 288, 562, and 571 of the PMAN structure, at which the conserved residues in the mesophilic and thermophilic mannanases are leucine, asparagine, arginine, tyrosine, glycine, threonine and serine (Table 4). The aromatic rings consists of a dipole that allows two favourable interactions including aromatic–aromatic interactions between aromatic rings at right angles to each other and aromatic-amino interactions between aromatic rings and the side chains of arginine and lysine. These interactions promote thermostability through an enthalpic contribution [45]. The comparison of the amino acid sequences of two homologous psychrophilic and mesophilic proteins revealed that the number of aromatic residues in psychrophilic proteins is more than that of the mesophilic counterpart. This indicates that some psychrophilic proteins need to maintain their 3D-fold in addition to their need for local structural flexibility to be active [51]. Psychrophilic enzymes adopt different strategies to increase their local and global flexibility and to be active in cold temperatures.

Glycine is also replaced in psychrophilic mannanases to regulate the entropy of the enzyme by increasing the flexibility of the molecule [52]. Because of the lack of a side chain, glycine has more conformational freedom to allow chain rotation [53]. Glycine substitution can be observed at positions 260, 324, 325, 378, 450, 491, 495 and 504 in the PMAN structure, at which they are conserved with other residues such as histidine, arginine, serine, lysine, asparagine, leucine, proline, valine, glutamine, and alanine (Table 4). The presence of glycine around the active site has been found to increase the flexibility of the active site [52]. Thus, substitution of alanine, isoleucine, cysteine, methionine and lysine with glycine at positions 373, 377, 378, and 456 in PMAN may improve the efficiency of the catalytic reactions of the psychrophilic PMAN and 2C0H.

Furthermore, several additional residue replacements were found in the multiple sequence alignment in Fig. 6. These include the substitution of large residues by smaller residues such as alanine among the same hydrophobic group at positions 243, 285, 336, and 404 of the PMAN structure, whereas the corresponding residues in mesophilic and thermophilic counterparts are other hydrophobic residues such as valine, glutamine, serine, isoleucine, and leucine. A previous comparative study on a lactate dehydrogenase from psychrophilic, mesophilic, and thermophilic *Bacillus* spp. [54] indicated that hydrophobic residues are substituted based on temperature from the more thermophilic valine, phenylalanine, isoleucine, and leucine to the more mesophilic and psychrophilic alanine and methionine. The charged amino acids glutamine and

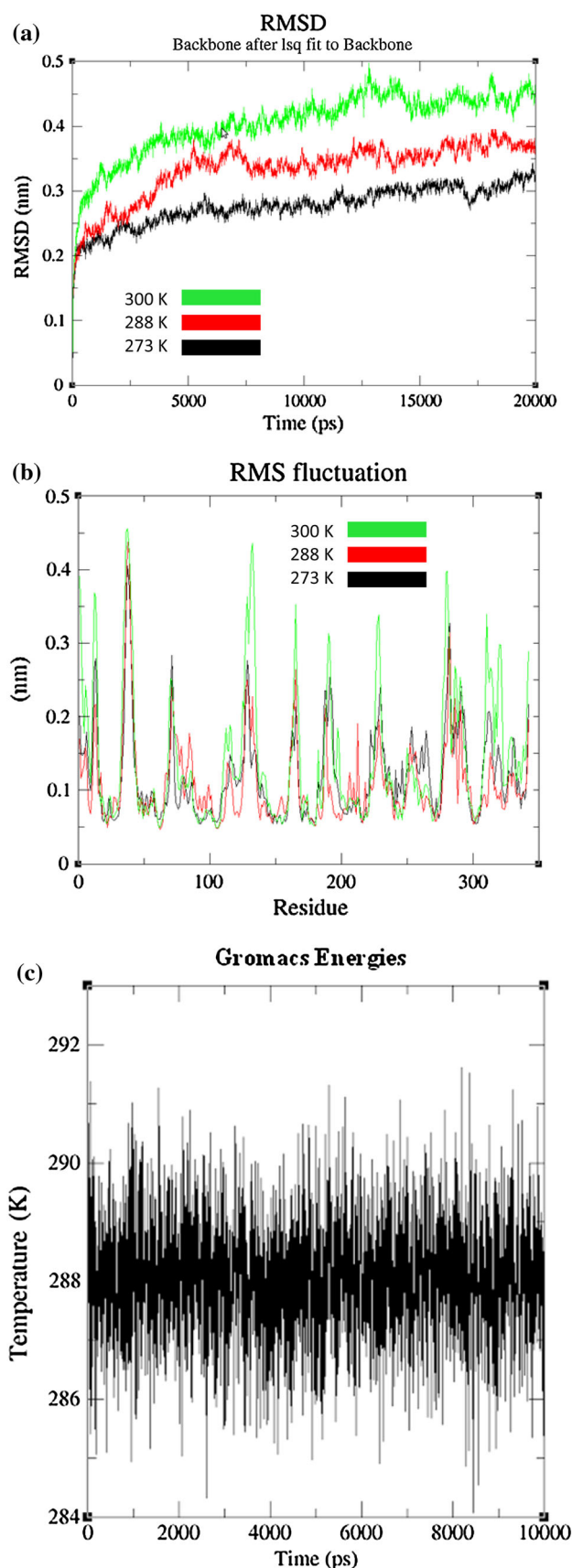


Fig. 7 Molecular dynamic simulation results: **a** RMSD for the main structure as the reference structure PMAN as a function of time at 273, 288 and 300 K, the optimum temperature of the simulation is at 288 K where it displays a more consistent RMSD value compared that of 273 and 300 K. **b** RMSF of the C $_{\alpha}$ atom of PMAN from the initial structure as a function of residue number at 273, 288 and 300 K, the structure simulated at 300 K generally show higher fluctuations compared with 273 and 288 K. **c** variation of the temperature during molecular simulation at 288 K

aspartate (mesophilic and thermophilic mannanases) are substituted with alanine at identical PMAN positions 233 and 237. These replacements reveal that the small hydrophobic alanine residue is more relevant in cold-loving enzymes in the production of proteins with high activity at low temperatures. In addition, the tyrosine, serine, phenylalanine, alanine, glutamine and valine that are present in mesophilic and thermophilic mannanase are replaced by threonine in PMAN at positions 183, 191, 229, and 427. This observation confirms the previous study that the cold-adapted archaea consists of fewer charged residues, and more hydrophobic amino acids such as alanine, and more noncharged polar residues such as threonine [55].

Energy minimisation, refinement and molecular dynamic simulation of PMAN

To minimise energy and improve the stability of the initial model structure, a molecular dynamics calculation was performed for 10 ns. The RMSD of the resulting structures relative to the starting structures were ~ 0.3 Å after 5 ns, and the RMSD value did not change significantly after 5 ns (illustrated in Fig. 7a). These RMSD values indicate that the employed simulation time was long enough to obtain an equilibrium structure for PMAN. Thus, the applied molecular dynamics was necessary to specify the geometry of PMAN. In addition, an average temperature of 10 ns simulation at 288 K for the studied system was equal to 288 ± 0.5 K (Fig. 7b). Therefore, the extracted equilibrium structure for PMAN at 288 K was obtained under stable temperature conditions.

However, in order to analyse the stability of the model, the constructed PMAN model was assessed by a molecular dynamic simulation at three different temperatures: 273, 288, and 300 K. Based on the RMSD analysis results at three different temperatures (Fig. 7c), the lowest value of RMSD was found at 273 K, followed by 288 and 300 K. From the figure, the simulation at 273 K was more stable in comparison with the simulation at 288 and 300 K. The RMSF of the C $_{\alpha}$ value of the PMAN structure at 273 K was comparable to the structure at 288 K, both of which are coil regions. At 300 K, the C $_{\alpha}$ of PMAN generally exhibited a higher fluctuation. A similar fluctuation pattern could be observed in the three simulations, with the highest

Table 5 Structural characteristics that are potentially effect on the stability of psychrophilic PMAN

Parameters	PMAN	3ZIZ	Expect effect on PMAN stability
Salt bridges (formed by arginine residues)	8	12	Ionic interactions decrease
Hydrogen bond	213	263	stability decrease
Accessible surface (Å ²)			
Hydrophobic accessibility	42.26 %	40.05 %	
Hydrophilic accessibility	43.17 %	38.22 %	
Surface of positively charged aa (basic)	9.11 %	11.78 %	
Surface of negatively charged aa (acidic)	5.46 %	9.95 %	

fluctuations occurring at the N terminus and in the loop between the secondary structure elements. The PMAN secondary structure fluctuations behaved similarly at all temperatures tested; higher fluctuations occurred in the loops, creating identical peak and groove signatures. The enhanced localised flexibility in the loop regions of PMAN confers a greater flexibility to the PMAN enzyme. A similar finding has been reported in a comparative molecular dynamics study of the psychrophilic and mesophilic anti-freeze proteins from *Macrozoarces mericanus* and humans, in which the localised flexibility in the loop region of the psychrophilic antifreeze protein at 277 and 298 K was greater than the flexibility in the mesophilic protein [56]. Therefore, this suggests that improved flexibility of the loop regions in PMAN could be a contributor to its adaptation to a cold environment. The evolution of the secondary structures during the MD simulation was determined by the database of secondary structure assignments (DSSP). Both simulations show that the global conformation of PMAN is stable with no significant changes in its secondary structure elements.

Comparative structural analysis of the cold adaptation of PMAN

Structural characteristics of the PMAN molecule were analysed to study its cold adaptation in comparison with the mesophilic β -mannanase from *P. anserina* (3ZIZ). Both the PMAN and mannanase from *P. anserina* are from the identical family with a similar TIM barrel fold. They also share common properties of mannanase enzymes. However, because of their adaptation to different temperatures, they are an acceptable set of homologous proteins to study for temperature adaptation. The structural characteristics that are potentially involved in the thermal stability of the molecule include the number of salt bridges, hydrogen

bonds, and the solvent interactions (such as hydrophobic, hydrophilic, positively, and negatively charged accessible surface areas) and were compared for both enzymes in Table 5.

Salt bridges are known as one of the important factors to stabilise protein structures. The disturbance of a salt bridge can directly influence the stability of a molecule [57]. Several previous studies using X-ray structure data revealed that cold adapted enzymes have a lower number of salt bridges [45]. The presence of arginine in the enzyme structure enhances the thermostability of a molecule by providing more electrostatic interactions through their guanidine group [58]. Based on the results in Table 5, the number of salt bridges in PMAN is lower than 3ZIZ; therefore, the structure of PMAN is thermally unstable. The PMAN structure consists of 8 arginine residues that form salt bridges compared to the 12 arginine residues in 3ZIZ that form salt bridges.

The psychrophilicity of the PMAN enzyme was further assessed by comparatively studying the accessible surface areas of the hydrophobic, hydrophilic, positively charged, and negatively charged amino acids. Based on the results in Table 5, the psychrophilic mannanase consists of an increased number of hydrophilic and hydrophobic accessible surface areas compared to the mesophilic mannanase. These differences enable the mesophilic mannanase to have improved electrostatic interactions to stabilise at higher temperatures. Psychrophilic enzymes tend to contain more hydrophobic residues in their accessible surface areas [45, 59]. This tendency increases the structural flexibility of the molecule at low temperatures as reported by Tronelli et al. [60]. The existence of hydrophobic residues on the surface of a protein destabilises its structure because of a decrease in the entropy of the water molecule. This decrease in water entropy creates cage-like structures around these residues. However, because of the decreased mobility of the released water molecules, the entropy is reduced at cold conditions [58].

In addition to the above factors, the psychrophilic mannanase consists of significantly fewer hydrogen bonds in comparison with its mesophilic counterpart. In the previous study by Tronelli [60], the role of this type of electrostatic interaction was demonstrated when assessing the higher stability of mesophilic and thermophilic enzymes. However, a satisfactory technique to confirm the role of the number of hydrogen bonds in the stability of the protein structure has not yet been proposed.

Conclusion

The results of this study provide quantitative evidence for a psychrophilic β -mannanase that displays several notable

adaptations to the cold environment. Structural differences on the surface of PMAN in the secondary structure and at the residue level contribute to the local flexibility of the structure in comparison with its mesophilic and thermophilic counterparts. This flexibility confirms the capability of this enzyme to function in cold environments. The predicted model for PMAN could be used in further comparative studies to correlate the characteristics of PMAN to other cold adapted proteins in nature. Additionally, these findings assist future efforts in the rational design of proteins with enhanced psychrophilic properties.

References

- Kokkinidis M, Glykos NM, Fadoulglou VE (2012) Protein flexibility and enzymatic catalysis. *Adv Protein Chem Struct Biol* 87:181–218
- Metpally RPR, Reddy BVB (2009) Comparative proteome analysis of psychrophilic versus mesophilic bacterial species: insights into the molecular basis of cold adaptation of proteins. *BMC Genomics* 10:11
- Liu Z, Qi W, He Z (2008) Optimization of beta-mannanase production from *Bacillus licheniformis* TJ-101 using response surface methodology. *Chem Biochem Eng Q* 22:355–362
- Wang M, You S, Zhang S, Qi W, Liu Z, Wu W, Su R, He Z (2013) Purification, characterization, and production of β -mannanase from *Bacillus subtilis* TJ-102 and its application in glucomannooligosaccharides preparation. *Eur Food Res Technol* 237:399–408
- Haiqiang L, Huitu Z, Pengjun S, Huiying L (2013) A family 5 β -mannanase from the thermophilic fungus *Thielavia arenaria* XZ7 with typical thermophilic enzyme features. *Appl Microb Biotechnol* 97:8121–8128
- Chantorn ST, Buengrisawat K, Pokaseam A, Sombat T, Dangpram P, Jantawon K, Nitisinprasert S (2013) Optimization of extracellular mannanase production from *Penicillium oxalicum* KUB-SN2-1 and application for hydrolysis property. *J Sci Technol* 35(1):17–22
- Ourgault R, Bewley JD (2002) Variation in its C-terminal amino acids determines whether endo-beta-mannanase is active or inactive in ripening tomato fruits of different cultivars. *Plant Physiol* 130(3):1254–1262
- Xu B et al (2002) Endo- β -1,4-Mannanases from blue mussel, *Mytilus edulis*: purification, characterization, and mode of action. *J Biotechnol* 92(3):267–277
- Davies G, Henrissat B (1995) Structures and mechanisms of glycosyl hydrolases. *Structure* 3:853–859
- El-Naggar MY et al (2006) Extracellular β -Mannanase production by the immobilization of the locally isolated *Aspergillus niger*. *Int J Agric Biol* 8(1):57–62
- Ehsani M, Torki M (2010) Effects of dietary inclusion of guar meal supplemented by β -Mannanase on performance of laying hens. *Egg Qual Charact Diacritical Count White Blood Cells* 5(4):237–243
- Zhou H, Yang Y, Nie X, Yang W, Wu Y (2013) Comparison of expression systems for the extracellular production of mannanase Man23 originated from *Bacillus subtilis* B23. *Microb Cell Fact* 12:78
- Lee JT, Bailey CA, Cartwright AL (2003) Beta-Mannanase ameliorates viscosity-associated depression of growth in broiler

- chickens fed guar germ and hull fractions. Poult Sci 82(12):1925–1931
14. Chandra M et al (2011) Isolation, purification and characterization of a thermostable β -Mannanase from *Paenibacillus* sp. DZ3. J Korean Soc Appl Biol Chem 54(3):325–331
 15. Tailford LE, Ducros VM-A, Flint JE, Roberts SM, Morland C, Zechel DL, Smith N, Bjørnvad ME, Borchert TV, Wilson KS, Davies GJ, Gilbert HJ (2009) Understanding how diverse beta-mannanases recognize heterogeneous substrates. Biochemistry 48:7009–7018
 16. Park SH, Park KH, Oh BC, Alli I, Lee BH (2011) Expression and characterization of an extremely thermostable B-glycosidase (mannosidase) from the hyperthermophilic archaeon *Pyrococcus furiosus* DSM 3638. N Biotechnol 28:639–648
 17. Goncalves AM, Silva C, Madeira T, Coelho R, Sanctis D, Romao MV, Bento I (2012) Endo- β -D-1,4-mannanase from *Chrysonilia sitophila* displays a novel loop arrangement for substrate selectivity. Acta Cryst D68:1468–1478
 18. Zhao Y, Zhang Y, Cao Y, Qi J, Mao L, Xue Y, Gao F, Peng H, Wang X, Gao G, Ma Y (2011) Structural analysis of alkaline β -Mannanase from alkaliphilic *Bacillus* sp. N16-5: implications for adaptation to alkaline conditions. PLoS ONE 6(1):e14608
 19. Santos CR, Squina FM, Navarro AM, Ruller R, Prade R, Murakami MT (2010) Cloning, expression, purification, crystallization and preliminary X-ray diffraction studies of the catalytic domain of a hyperthermostable endo-1,4- β -D-mannanase from *Thermotoga petrophila* RKU-1. Acta Cryst F66:1078–1081
 20. Akita M, Takeda N, Hirasawa K, Sakai H, Kawamoto M, Yamamoto M, Grant WD, Hatada Y, Ito S, Horikoshi K (2004) Crystallization and preliminary X-ray study of alkaline mannanase from an alkaliphilic *Bacillus* isolate. Acta Cryst D60:1490–1492
 21. Sabini E, Schubert H, Murshudov G, Wilson KS, Siika-Aho M, Penttilä M (2000) The three-dimensional structure of a *Trichoderma reesei* beta-mannanase from glycoside hydrolase family 5. Acta Cryst D56:3–13
 22. Larsson AM, Anderson L, Xu B, Munoz IG, Uson I, Janson JC, Stalbrand H, Stahlberg J (2006) Three-dimensional crystal structure and enzymic characterization of β -mannanase Man5A from blue mussel *Mytilus edulis*. J Mol Biol 357:1500–1510
 23. Bourgault R et al (2005) Three-dimensional structure of (1,4)- β -D-mannan mannanohydrolase from tomato fruit. Protein Sci 14:1233–1241
 24. Zakaria MM, Yamamoto S, Yagi T (1998) Purification and characterization of an endo-1,4- β -mannanase from *Bacillus subtilis* KU-1. FEMS Microbiol Lett 158:25–31
 25. Huang JW, Chen CC, Huang CH, Huang TY, Wu TH, Cheng YS, Ko TP, Lin CY, Liu JR, Guo RT (2014) Improving the specific activity of β -mannanase from *Aspergillus niger* BK01 by structure-based rational design. Biochimica et Biophysica Acta (BBA) Proteins and Proteomics 1844(3):663–669
 26. Ramli ANM et al (2011) Molecular cloning, expression and biochemical characterisation of a cold-adapted novel recombinant chitinase from *Glaciozyma antarctica* PI12. Microb Cell Fact 10(1):94
 27. Altschul SF et al (1997) Gapped BLAST and PSI-BLAST: a new generation of protein database search programs. Nucleic Acid Res 25(17):3389–3402
 28. Altschul SF et al (1990) Basic local alignment search tool. J Mol Biol 215(3):403–410
 29. Gough J et al (2001) Assignment of homology to genome sequences using a library of hidden Markov models that represent all proteins of known structure. J Mol Biol 313(4):903–919
 30. Fornes O et al (2009) ModLink+: improving fold recognition by using protein–protein interactions. Bioinformatics 25(12):1506–1512
 31. Söding J, Biegert A, Lupas AN (2005) The HHpred interactive server for protein homology detection and structure prediction. Nucleic Acid Res 33(2):W244–W248
 32. Jones DT (1999) An efficient and reliable protein fold recognition method for genomic sequences. J Mol Biol 287(4):797–815
 33. Kelley LA, Sternberg MJE (2009) Protein structure prediction on the web: a case study using the Phyre server. Nat Protoc 4(3):363–371
 34. Eswar N et al (2007) Comparative protein structure modeling using MODELLER. Curr Protoc Bioinformatics 2(1):1–30
 35. Zhang Y, Skolnick J (2005) TM-align: a protein structure alignment algorithm based on the TM-score. Nucleic Acid Res 33(7):2302–2309
 36. Luthy R, Bowie JU, Eisenberg D (1992) Assessment of protein models with three-dimensional profiles. Nature 356(6364):83–85
 37. Laskowski RA et al (1993) PROCHECK: a program to check the stereochemical quality of protein structures. J Appl Crystallogr 26(2):283–291
 38. Colovos C, Yeates TO (1993) Verification of protein structures: patterns of nonbonded atomic interactions. Protein Sci 2(9):1511–1519
 39. Wiederstein M, Sippl MJ (2007) ProSA-web: interactive web service for the recognition of errors in three-dimensional structures of proteins. Nucleic Acid Res 35(2):W407–W410
 40. Hess B et al (2008) GROMACS 4: algorithms for highly efficient, load-balanced, and scalable molecular simulation. J Chem Theory Comput 4(3):435–447
 41. Couturier M, Roussel A, Rosengren A, Leone P, Stalbrand H, Berrin JG (2013) Structural and biochemical analyses of glycoside hydrolase families 5 and 26 β -(1,4)-mannanases from *Podospora anserina* reveal differences upon manno-oligosaccharide catalysis. J Biol Chem 288:14624
 42. Costantini S, Colonna G, Facchiano AM (2008) ESBRI: a web server for evaluating salt bridges in proteins. Bioinformatics 3(1):137–138
 43. Pettersen E et al (2004) UCSF Chimera—a visualization system for exploratory research and analysis. J Comput Chem 25(13):1605–1612
 44. Chaitanya M et al (2010) Exploring the molecular basis for selective binding of *Mycobacterium tuberculosis* Asp kinase toward its natural substrates and feedback inhibitors: a docking and molecular dynamics study. J Mol Model 16(8):1357–1367
 45. Geralt M, Alimenti C, Vallesi A, Luporini P, Wuthrich K (2013) Thermodynamic stability of psychrophilic and mesophilic pheromones of the protozoan ciliate euplotes. Biology 2:142–150
 46. Alvarez M et al (1998) Triose phosphate isomerase (TIM) of the psychrophilic *Bacterium* *Vibrio marinus*. J Biol Chem 273:2199–2206
 47. Wallon G et al (1997) Sequence and homology model of 3-isopropylmalate dehydrogenase from the psychrotrophic bacterium *Vibrio* sp. I5 suggest reasons for thermal instability. Protein Eng 10(6):665–672
 48. Davail S et al (1994) Cold adaptation of proteins. Purification, characterization, and sequence of the heatlabile subtilisin from the antarctic psychrophile *Bacillus* TA41. J Biol Chem 269(26):17448–17453
 49. Herning T et al (1992) Role of proline residues in human lysozyme stability: a scanning calorimetric study combined with X-ray structure analysis of proline mutants. Biochemistry 31(31):7077–7085
 50. Kumar S, Nussinov R (2004) Different roles of electrostatics in heat and in cold: adaptation by citrate synthase. Chem Biochem 5(3):280–290
 51. Alimenti C et al (2009) Molecular cold-adaptation: comparative analysis of two homologous families of psychrophilic and

- mesophilic signal proteins of the protozoan ciliate, *Euplotes*. IUBMB Life 61(8):838–845
52. Galkin A et al (1999) Coldadapted alanine dehydrogenases from two Antarctic bacterial strains: gene cloning, protein characterization, and comparison with mesophilic and thermophilic counterparts. Appl Environ Microbiol 65(9):4014–4020
53. Kim SY et al (1999) Structural basis for cold adaptation. J Biol Chem 274(17):11761–11767
54. Zuber H (1988) Temperature adaptation of lactate dehydrogenase. Structural, functional and genetic aspects. Biophys Chem 29(1–2):171–179
55. Saunders N et al (2003) Mechanisms of thermal adaptation revealed from the genomes of the antarctic archaea *Methanogenium frigidum* and *Methanococcoides burtonii*. Genome Res 13(7):1241–1255
56. Kundu S, Roy D (2009) Comparative structural studies of psychrophilic and mesophilic protein homologues by molecular dynamics simulation. J Mol Graph Model 27(8):871–880
57. Kumar S, Nussinov R (1999) Salt bridge stability in monomeric proteins. J Mol Biol 293(5):1241–1255
58. Ramli ANM, Mahadi NM, Shamsir MH (2012) Structural prediction of a novel chitinase from the psychrophilic *G. antarctica* PI12 and an analysis of its structural properties and function. J Comput Aided Mol Des 26:947–961
59. Bae E, Phillips G (2004) Structures and analysis of highly homologous psychrophilic, mesophilic, and thermophilic adenylate kinases. 279(27):28202–28208
60. Tronelli D et al (2007) Structural adaptation to low temperatures—analysis of the subunit interface of oligomeric psychrophilic enzymes. FEBS J 274(17):4595–4608